Thermomechanical and viscoelastic properties of green composites of PLA using chitin micro-particles as fillers

Mohammad M Hassan[1,2,*] · Kiyohito Koyama[1,3]

ABSTRACT

Many thermoplastic biocomposites made with non-biodegradable polymers as a matrix polymer are not biodegradable. In this work, biodegradable polylactide (PLA)/chitin micro-particle composites were successfully prepared by melt blending without using any compatibilizer or processing aid. The effects of the addition of chitin micro-particles to PLA on its thermal stability, physicomechanical properties and microstructures were evaluated by thermo-gravimetric analysis, dynamic mechanical thermal analysis, differential scanning calorimetry, tensile strength measurement, and scanning electron microscopy. It was found that the addition of chitin micro-particle to PLA increased the stiffness, tensile strength, and hydrophobicity of PLA but negatively affected its thermal properties and elongation. The tensile strength exhibited by the pristine PLA was 41.5 MPa, which increased to 48.5 for the chitin loading of 3% but a further increase in the chitin loading resulted in a reduction in tensile strength. The increase in chitin loading resulted in an increase in stiffness of PLA as

---

* Mohammad Mahbubul Hassan
  mahbubul.hassan@agresearch.co.nz

[1] Venture Business Laboratory, Yamagata University, 4-3-16 Jonan, Yonezawa, Yamagata   Prefecture, Japan.

[2] Bioproduct & Fiber Technology Team, AgResearch Limited, 1365 Springs Road, Lincoln 7647, New Zealand.

[3] Department of Polymer Science & Engineering, Yamagata University, 4-3-16 Jonan, Yonezawa, Yamagata Prefecture, Japan.

the storage increased from 3.21 GPa for the neat PLA to 3.48 GPa for the PLA loaded with 3% chitin microparticles. The results show that chitin can be used for the reinforcement and also to enhance the moisture barrier properties of PLA.

Key-Keywords: PLA biocomposites; chitin, thermal analysis, viscoelastic properties; mechanical properties

Introduction

Fiber-reinforced composites (FRC) are used in many applications including automobile parts, wind turbines, building constructions, and packaging [1-3]. However, most of the FRCs currently being used (such as glass fiber/polyester and glass fiber/epoxy), are made from petroleum-based polymers that virtually do not biodegrade. According to the European Association of Plastics Recycling and Recovery (EPRO) data, only 34.7% of all the plastic packaging waste is recycled [4] and the rests are incinerated as solid waste. Accumulation of plastics in the environment and their possible effects on aquatic and terrestrial ecology are drawing media attention [5, 6]. The problem of growing global waste and their disposal is driving the development of FRCs from renewable and sustainable biodegradable polymers. The ever-stringent legislations and consumers' demand forced the plastic manufacturers to consider the environmental impact of their products at all stages, from production to the after-use-disposal.

Over the years, a range of biodegradable polymers has been developed including polylactic acid [7], polycaprolactone [8], polybutylene succinate [9], polyhydroxy butyrate [10], and poly(hydroxybutyrate-co-valerate) [11] for various applications. Of the biodegradable polymers developed until the present, polylactide (PLA) shows the greatest promise because

of its environmental sustainability, and high strength. PLA is made from lactide by ring-opening polymerization and lactide is made from natural polysaccharides by fermentation in different stages. As a thermoplastic polymer, PLA can be processed like other thermoplastic polymers, such as polyolefins, polyamides, and polyesters by injection molding [12], film extrusion [13], blow molding [14], and 3D printing [15]. However, PLA does not biodegrade as fast as natural polymers but degrades over a period of several months to two years compared to other petroleum-based thermoplastics needing decades [16].

Despite its many advantages, still, PLA has several demerits, such as brittleness, poor toughness, poor impact strength, and poor gas and moisture barrier properties [17]. It is known that by the addition of a few percents of nano to micro-sized particles, the tensile strength of thermoplastic polymers can be considerably increased [18, 19]. It was reported that the addition of cellulose nanocrystals to PLA increased its toughness and biodegradability [20]. The addition of 5% maleic anhydride-modified cellulose microfibril to PLA increased its crystallization up to 100 °C [21].

The bio-based fillers investigated for the manufacturing of fully biodegradable PLA composites are mostly hydrophilic. PLA is a hydrophobic polymer and therefore these bio-based fillers are incompatible to PLA. For the manufacturing of bio-based filler-reinforced-PLA composites, either hydrophilic groups will need to be introduced in PLA, which may further affect its poor moisture and gas barrier properties, or the fillers will need to be hydrophobically modified to make them compatible, which is an extra step that increases the manufacturing cost of the composites [22–24]. Moreover, chemical modification of fillers or PLA also may affect the biodegradability of the produced bio-composites. For example, it was reported that starch films and sheets grafted with poly(methacrylic acid) and polycaprolactone only partial biodegraded in the soil burial test whereas ordinary starch film fully biodegraded [25, 26]. Similarly, the grafting of natural flax fiber with polyethylene

glycol slowed down flax fiber's biodegradability [27]. Chitin is a natural biodegradable polysaccharide polymer having hydrophobic acetyl amide groups and therefore should be compatible with hydrophobic PLA. Recently Singh et al. reported that the addition of chitin nanocrystals to the triethyl citrate compatibilized-PLA increased the tensile strength and elongation of the produced PLA/chitin nanocrystal nanocomposite [28]. Mahmoodi et al. reported that the addition of a small weight(%) of organic dye-modified-nanoclay to PLA improved the tensile strength, photo-protection capability, and moisture vapor permeability of PLA [29]. Lertphirun and Srikulkit found that the addition of hydrophobic silane-modified cellulose to PLA reduced the moisture vapor permeability of PLA [30]. However, chitin has not been considered for the reinforcing and increasing the moisture vapor barrier properties of PLA.

In this work, PLA/chitin micro-particle biocomposites were successfully prepared by melt blending at 150 °C in a Brabender-type static mixer without using any compatibilizer, plasticizer or processing aid. The prepared composites were characterized by thermal differential scanning calorimetry, thermogravimetric analysis, dynamic mechanical analysis and scanning electron microscopy. To the best of our knowledge, no published literature reported the preparation of PLA/chitin microparticle biocomposites by melt blending without using any compatibilizer and the effect of chitin on the physicochemical characteristics of PLA.

Experimental

Materials

The PLA in pellet form with a molecular weight of M_n = ~60000, specific gravity 1.24 g/cm^3, and MFR = 6 g/10 was purchased from Sigma-Aldrich Chemicals (USA). Chitin micro-particles of an average length of 100 µm were purchased from Sigma-Aldrich Chemicals (USA).

Preparation of PLA/chitin composites

PLA pellets and chitin micro-particles were dried at 80 °C for 24 hours under vacuum to remove the absorbed moisture. The PLA/chitosan composites were prepared by manually mixing the pre-weighed quantities of PLA and the chitin microparticles by melt compounding at 160 °C for 10 min under the nitrogen environment using a static mixer (Labo Plastomil, Model 655, Toyo Seiki Seisaku-sho, Inc., Japan) without using any compatibilizer or processing aid. The screw speed was maintained at 90 rpm. The application levels of chitin microparticles were varied from 1 to 3 weight%. The chitin microparticles were dispersed in the PLA matrix by melt blending them for 10 min as the torque graph showed that 10 min mixing was sufficient for the optimum homogeneous mixing of chitin particles with PLA. The PLA/chitin composite samples were pelletized to 2 mm long pellets.

Thermal analysis

The non-isothermal crystallization and the subsequent melting behavior of neat PLA and its composites were examined on a Perkin-Elmer 7 differential scanning calorimeter (DSC) equipped with an intercooler, which was calibrated with metallic indium (99.9% purity). The samples were heated from room temperature to 200 °C at the rate of 10 °C/ min and held for 5 min, then cooled to 0 °C at 10 °C/min and held for 5 min, and again heated to 200 °C at 10

°C/min to minimize the effect of static heat. The second heating curve was used for the DSC analysis of the various PLA/chitin blends.

Thermogravimetric analysis (TGA) is a tool to assess the thermal stability of polymers. TGA curves were recorded on a Seiko DSC/TG analyzer (Model SSC 5000, Seiko Instruments Inc., Japan) at room temperature to 500°C at a heating rate of 10 °C/min under nitrogen environment. All TGA runs employed nitrogen (99.99% pure and food grade) as a purge gas for the furnace with a constant flow rate of 100 ml/min. For each run, 10 mg of the sample of neat PLA or PLA/chitin composites was loaded in a platinum pan and heated to 500 °C at a linear rate of 10° C/min under constant nitrogen gas flow (100 ml/min). The thermogravimetric (TG) curves and differential thermal analysis curves were recorded simultaneously along with the temperature rise.

Dynamic mechanical analysis (DMA) was carried out to measure the stiffness and storage moduli of PLA and PLA/chitin composites as a function temperature. To carry out DMA analysis, $13 \times 56 \times 1.5$ mm size samples of neat PLA and PLA composites with various chitin micro-particle loading were prepared by compression molding at 160 °C for 10 min at 10 MPa pressure and then cooled under the same pressure by using a fan. In this work, DMA was carried out on a Rheometric Scientific DMA machine (Model RSA3, Rheometric Scientific, Piscataway, USA). The measurements were carried out in the dynamic time sweep test starting from $T = 25$ °C to 80 °C at the heating rate of 5°C/min and the frequency was fixed at 1 Hz and shear strain at 0.15%. The storage modulus, loss modulus and loss factor (tan δ) of the samples were measured.

Tensile tests

1.5 mm thick dog-bone plates were prepared by compression molding (Mini Hot Press, Toyo-Seiki Seisaku-sho) at 170 °C for 5 min at 10 MPa pressure and then slow cooling under the pressure of 10 MPa to facilitate crystallization. Tensile tests were performed to examine tensile strength or breaking force and elongation according to the ASTM standard test method DD638-03. The tensile strength was measured by the Instron Universal Tensile testing machine (Model 4404, Instron Inc., USA). The gauge length and the crosshead speed were 50 mm and 20 mm/min respectively. An extensometer was employed to determine the elongation of the samples. Tests were carried out in an environmentally conditioned room maintained at 20 ± 1°C and 65 ± 1% RH. The samples were preconditioned at those conditions for 48 h before measuring. The 10 identical samples of each blend composition and the control were measured, and the average values are reported here.

Surface morphologies

The morphology of chitin micro-particles was examined by a field emission scanning electron microscope (FESEM) at 10 kV without gold coating. In the case of neat PLA and its composites with chitin, $100 \times 10 \times 1.5$ mm size plates were placed in liquid nitrogen and then fractured by impact with a hammer. The fractured surfaces were scanned in a JEOL SEM at 15 kV. The surfaces of various composites were examined by a light microscope (Model: BX61, Olympus Corporation, Tokyo, Japan) equipped with a digital camera interfaced to a personal computer.

Water absorption

To evaluate the effect of the addition of chitin particles to PLA on its moisture barrier properties, water absorption test was carried out according to the ASTM D570 method. 4 cm $\times$ 4 cm $\times$ 4 cm size samples were immersed in distilled water at room temperature, after which they were removed from the tank at 10, 20, 30, 60, and 240 min, wiped by tissue paper, and weighed. The samples were again immersed in the water after each measurement. Finally, the water uptake was calculated as the mass difference and expressed as a percentage.

Fourier transform infrared spectroscopy

1 mm thick films of neat PLA and PLA/chitin composites were scanned on a Fourier transform infrared spectrometer with an attenuated total reflectance attachment (ATR-FTIR) using a ZnSe crystal. The wavelength cut off was below 650 cm^{-1}. The ATR-FTIR used was a Shimadzu FT-IR (Model: Prestige 21, Shimadzu Corporation, Tokyo, Japan). 64 scans were signal-averaged and reported here.

Results and discussion

Characterization of chitin microparticles

Figure 1(a) shows the SEM image of the chitin microparticles used in this work. It is evident that chitin particles are in micrometer size thin flake form with various geometrical shapes. The flakes are also in layered form and in each flake, several layers are bound together. The flakes are quite irregular in shape, and there is debris of chitosan flakes of sizes even less than 10 µm are visible in the SEM micrographs.
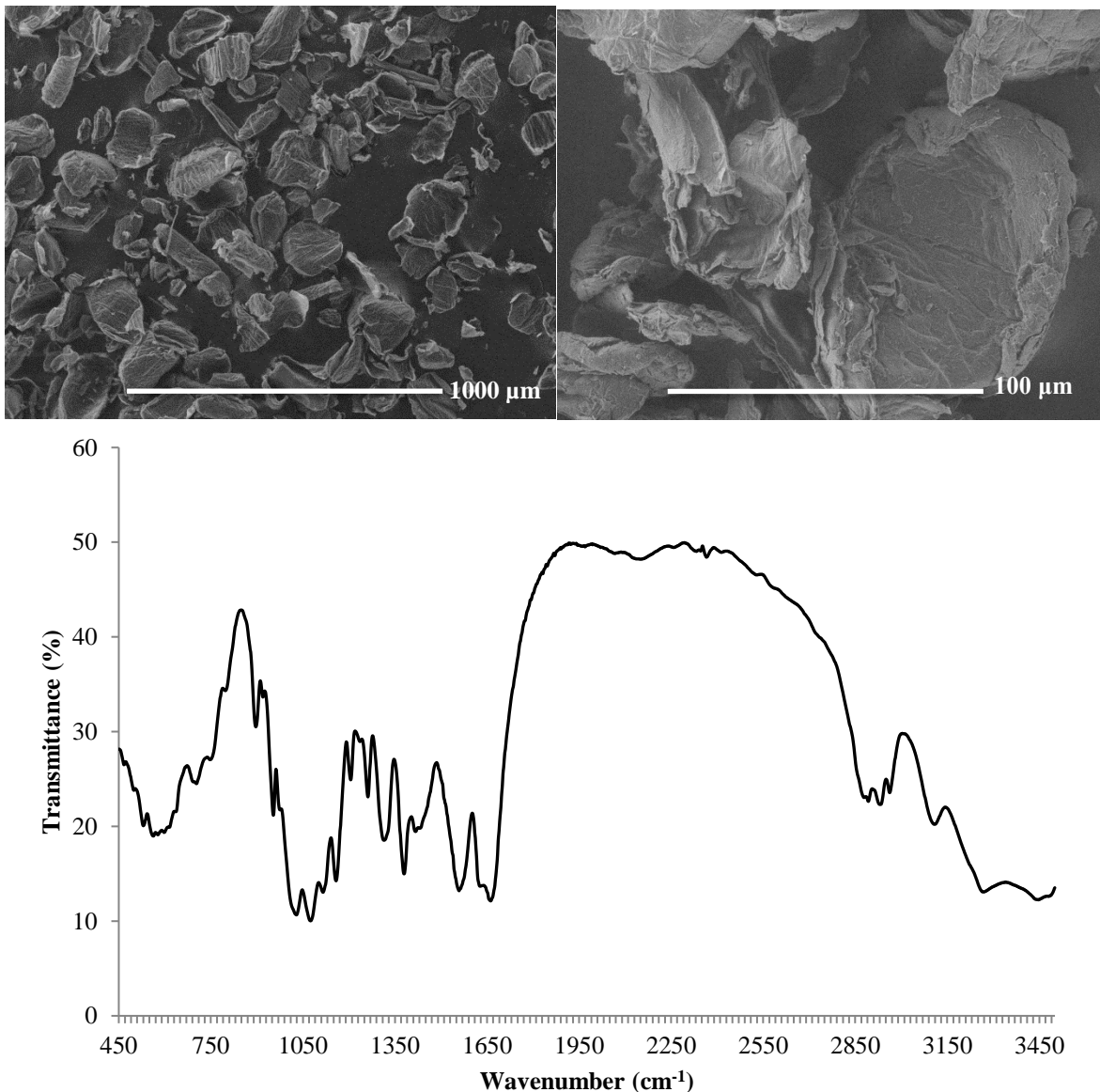
Figure 1   SEM micrographs (top) and FTIR spectrum (bottom) of chitin.

Figure 1(b) shows the FT-IR spectrum of chitin, which is consistent with the FT-IR spectrum of chitin shown in other published literature [31, 32]. The spectrum of chitin shows the usual characteristic peak at 2930 and 2962 cm^{-1} that can be assigned to stretching vibration of CH_2 and CH_3 respectively [33]. The broad band at 3450 cm^{-1} can be assigned to hydroxyl groups of chitin. The other major bands at 1320, 1550, 1660 cm^{-1} can be due to the presence of amide (III), amide (II) and amide (I) respectively. The IR absorption band at

1380 cm^{-1} is due to the symmetric deformation of methyl groups of chitin. The bands at 1032, 1073 and 1108 cm^{-1} are due to the stretching vibrations of C–O and the band at 1157 cm^{-1} is due to the stretching vibration of C–O–C. The band at 1265 cm^{-1} is due to the presence of –NH in chitin. The bands at 895 and 952 cm^{-1} represent CH and CH$_3$ groups respectively.
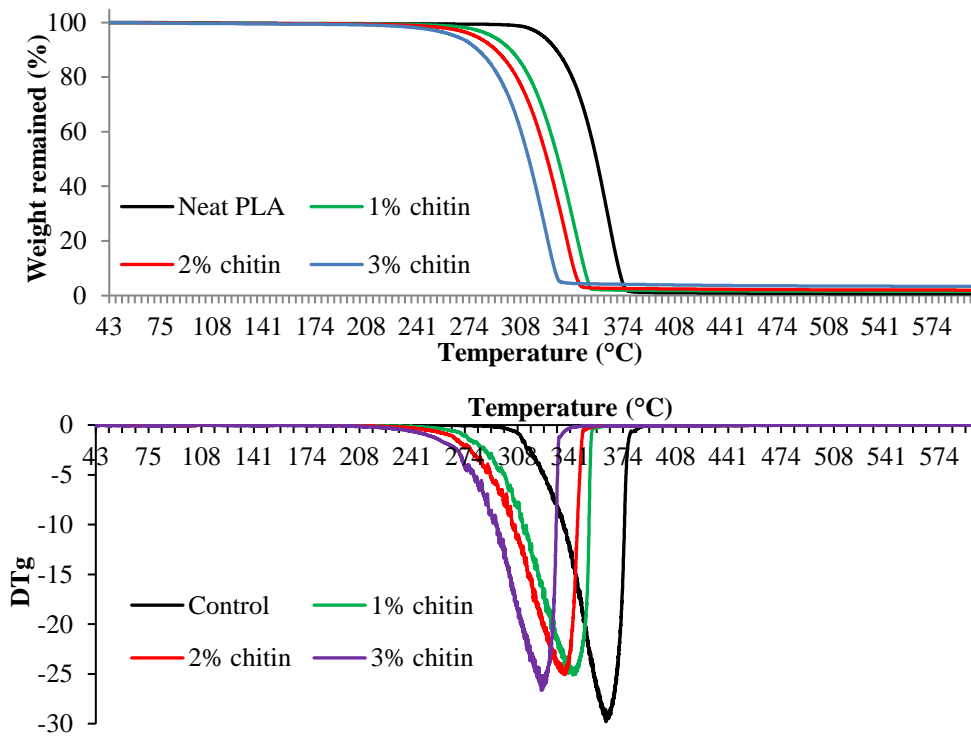

Figure 2   TGA (top) and DTG (bottom) curves of neat PLA and PLA/chitin composites with various weight (%) of chitin.

Thermogravimetric analysis

The TGA curves of neat PLA and PLA with various weight% of chitin is shown in Figure 2. The TGA curves show that the addition of chitin to PLA reduced the thermal stability of PLA. In the TGA, the weight loss of PLA and chitin were monitored, which occurred due to the formation of volatiles by the decomposition of the matrix polymer and the fillers. For all

samples, the weight loss occurred at four stages except for the neat PLA, for which the weight loss occurred at three stages. For neat PLA, the weight loss occurred at 280–320, 320–375 and 375–600 °C. Very little weight loss (approx. 0.6%) was observed up to 280 °C due to the loss of moisture as PLA hardly absorbs any moisture. However, a rapid weight loss was observed in the second stage as the weight loss increased from 0.6% to 97.2% at 375 °C due to the degradation and depolymerization of PLA. Further weight loss was observed up to 600 °C.

Table 1   The temperatures at which 10% and 80% weight loss occurred, and also the peak degradation temperatures and char yields of neat PLA and PLA/chitin biocomposites containing various chitin loading.

Materials	T_{10} (°C)	T_{80} (°C)	T_{peak} ((°C)	Char yield (%)
Neat PLA	330.7	367.3	363.0	0.64
PLA/1% chitin	301.1	344.5	339.9	1.47
PLA/2% chitin	291.7	337.8	337.5	1.99
PLA/3% chitin	280.0	325.3	323.0	3.20

However, for the PLA/chitin composites the weight loss occurred at 67–113, 113–230, 230–362 and 362–600 °C for 1% chitin, 67–113, 113–220, 220–355, and 355–600 °C for 2% chitin, and 67–113, 113–198, 198–341, 341–600 °C for 3% chitin respectively. The TGA curves for the first stage heating cycle reveals that the addition of chitin to the PLA had little effect on the moisture content of PLA as the weight loss at this stage due to the loss of absorbed moisture was similar for the neat PLA and PLA/chitin composites with various PLA loadings. The weight loss in the second stage for all the samples is very low compared to the first stage as chitin shows quite good thermal stability from 113-230 °C. In the third stage, a rapid loss in weight occurs for neat PLA and PLA/chitin composites as the

degradation of PLA and chitin occurs at this stage. Again, in the 4th stage, the weight loss was slowed down.

The TGA results of neat PLA and PLA/chitin composites are summarized in Table 1. The temperature at which 10% (T_{10}) and 80% (T_{80}) weight loss occurred for the control is 330.7 and 367.3 °C respectively. However, the T_{10} and T_{80} temperature for the PLA/chitin composites decreased with an increase in the weight (%) of chitin. The peak degradation temperature peak (T_{max}) measured from the DTG curve showed that the T_{max} for the control is 363.0 °C, which decreased with an increase in the weight (%) of chitin and decreased to 323.0 °C for the PLA containing 3% loading of chitin. It is quite interesting to know that although the peak degradation temperature decreased, the char yield increased with an increase in the weight (%) of chitin. The results suggest that at over 325 °C produced degradation product of chitin that was not further degraded with an increase in temperature, whereas PLA almost fully degraded.

Differential scanning calorimetry

The second heating DSC curves shown in Figure 3 illustrate the phase transition of PLA/chitin composites as a function of temperature and the derived transition temperatures are tabulated in Table 2. The thermogram of neat PLA and PLA/chitin composites showed three thermal transitions, such as glass transition (T_g), melting (T_m), and crystallization (T_c) temperatures. The neat PLA showed T_g at 58.5 °C, but the addition of chitin to PLA slightly decreased its T_g, which decreased with an increase in the chitin loading in the PLA/chitin composites. The T_g decreased from 58.5 °C to 56.3 °C for the composites containing 3% chitin. The neat PLA showed an exothermic cold crystallization peak (T_c) at 111.2 °C for recrystallization. The exothermic peak shown by the neat PLA at 111.2 °C moved to 111.8,

111.3 and 111.1 °C for the PLA/chitin composites with 1, 2, and 3% chitin loading. The small decrease in T_c was contributed by the nucleating effect of chitin microparticles that led to faster recrystallization [34]. The small change in T_c indicates that the addition of chitin plays a role in reducing the crystallization rate.

Table 2   Thermal properties of neat PLA and PLA/chitin composites with various PLA loading.

Materials	T_g (°C)	T_{cc} (°C)	T_{m1} (°C)	T_{m2} (°C)
Neat PLA	58.5	111.2	146.8	-
PLA/chitin (99/1 w/w)	56.9	112.0	145.8	152.03
PLA/chitin (98/2 w/w)	56.5	112.1	145.7	153.1
PLA/chitin (97/3 w/w)	56.3	111.0	145.4	153.3

The recrystallized PLA started to melt and produced an endothermic peak at 146.4 °C attributed to imperfect crystallinity. The control PLA showed just one melting peak, but the PLA/chitin composites showed two melting peaks, which is consistent with the published data [35]. The first melting peak started decreasing but the second melting peak started increasing with the increase in the chitin loading in the composites. The addition of chitin microparticles to PLA slightly affected the T_g of PLA but produced a second melting peak, which increased with an increase in the loading of chitin microparticles in the PLA/chitin composites.
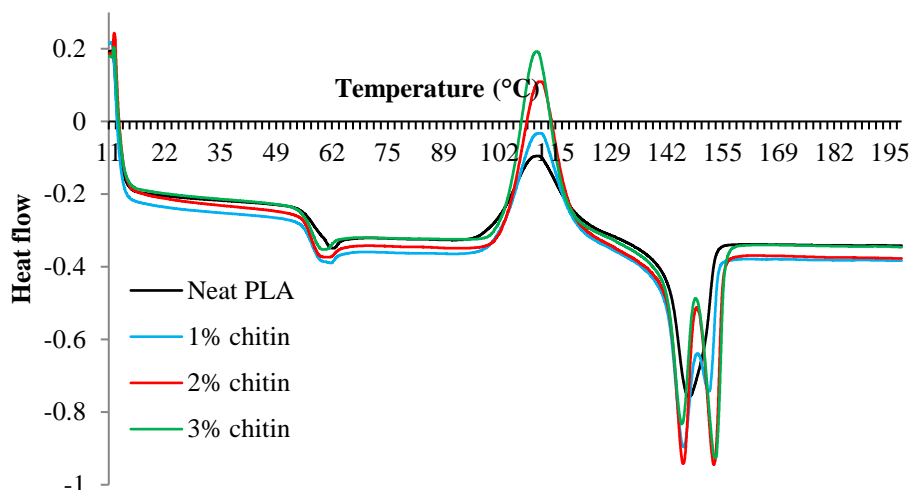
Figure 3   DSC thermograms (second run) of neat PLA and also PLA with 1, 2 and 3 chitin loading.

Dynamic mechanical analysis

The dynamic mechanical analysis was carried out to determine the effect of the addition of chitin microparticles to PLA on the stiffness of the PLA, and to understand its viscoelastic behavior over various temperatures. Figure 4 shows the effect of the addition of various weight (%) of chitin to PLA on its storage modulus (E') and loss modulus (E'') at various temperatures. It is evident that the addition of chitin particles to PLA increased the storage modulus of the composites, which increased with an increase in the chitin loading in the PLA/chitin biocomposites. The addition of 1% chitin showed a marginal effect on the storage modulus of the PLA up to the highest tested temperature but a further increase in the PLA loading considerably affected the storage modulus of PLA up to the glass transition temperature of PLA (58 °C), and beyond that temperature, very little effect was observed. At 30 °C, the storage modulus of the neat PLA was 3.21 GPa, which increased to 3.37 and 3.48 GPa for the chitin loading of 2 and 3% respectively. Figure 4 also shows the loss modulus of

PLA/chitin biocomposites containing various chitin loading. The loss modulus accounts for the viscous component of the complex modulus or the out of phase component with the applied strain, which normally increases with an in the weight% of PLA. The loss modulus also increased with an increase in the weight (%) of chitin in the PLA/chitin biocomposites, but the greatest effect was observed for the 3% chitin loading. It can be concluded that the addition of chitin to PLA, especially at 3% loading, considerably increased the stiffness of PLA.
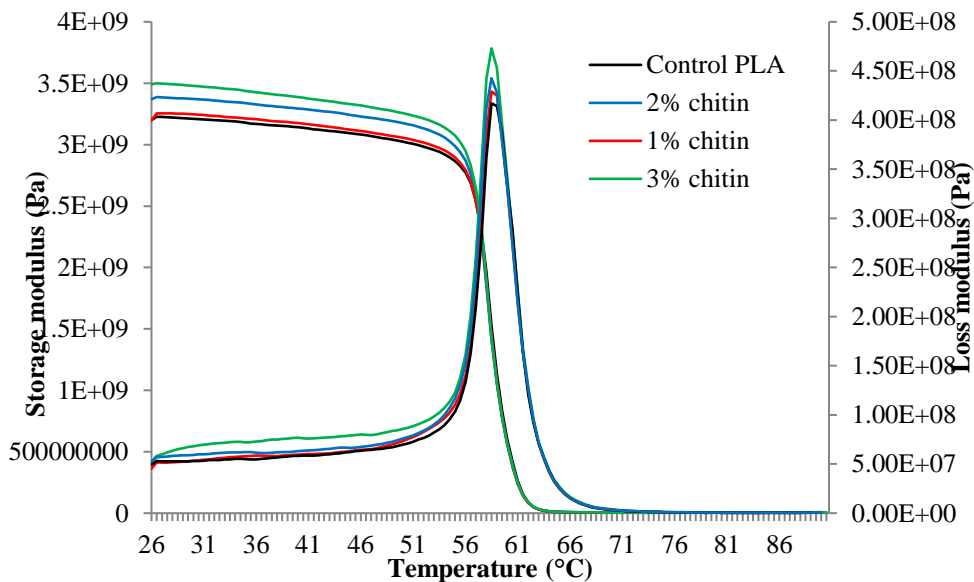

Figure 4   Storage and loss moduli of neat PLA and PLA/chitin composite containing various weight (%) of chitin microparticles.

Effect of addition of chitin microparticles on mechanical loss factor of PLA//chitin composites

Tan δ is a damping term that can be related to the phase transitions. The effect of mechanical loss factor, Tan δ, on chitin volume fraction as a function of temperature at a frequency of 1 Hz is shown in Figure 5. The control shows a sharp Tan δ peak at 64 °C, which is associated with the glass transition temperature (T_g) of PLA. The increase of chitin loading did not move Tan δ peak indicating that the addition of chitin microparticles did not cause any change in the phase transition behavior of PLA. However, the peak height of Tan δ decreased with an increase in the weight (%) of chitin as the increase in loading of the chitin micro-particles to PLA progressively decreased the molecular motion of PLA macromolecular chains, i.e. decreased damping properties.
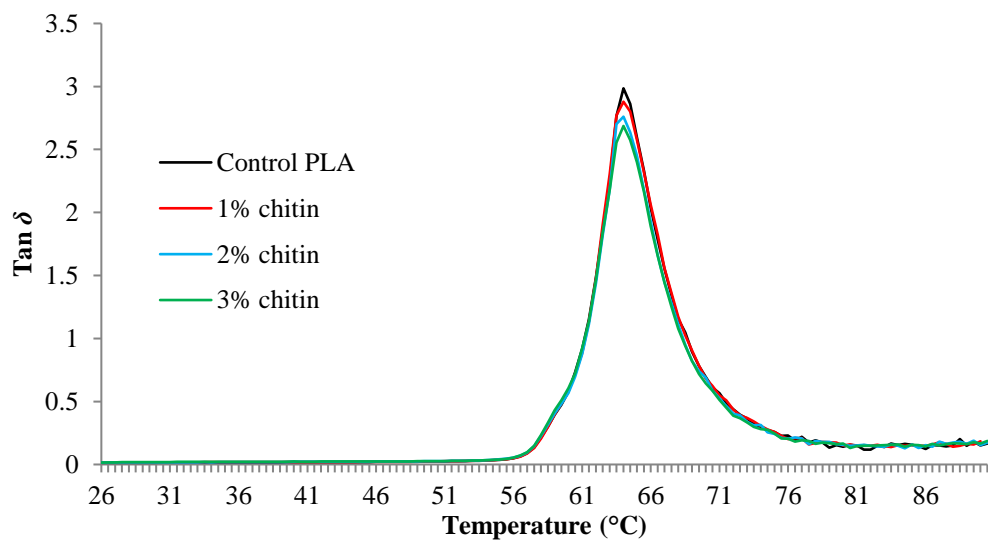

Figure 5   Effect of the weight (%) of chitin microparticles on the damping and glass transition temperature of neat PLA and PLA composites.

Mechanical properties

The mechanical properties of neat PLA and its composites with chitin microparticles are summarized in Table 3. The addition of chitin microparticles showed effectiveness as a

reinforcing agent in increasing the tensile strength of PLA/chitin composites. The tensile strength shown by control PLA was 41.5 MPa, which increased to 44.3 MPa for the PLA containing 1% chitin micro-particles. The tensile strength of PLA increased to the maximum 48.9 MPa for the chitin micro-particle loading of 3% and beyond that level, the tensile strength started decreasing. However, the elongation decreased with an increase in the chitin loading due to interactions between chitin and PLA, which reduced the movement of molecular chains of PLA. The increase in tensile strength suggests that the chitin microparticles was compatible with PLA probably due to the formation of hydrophobic-hydrophobic interactions.

Table 3   The effect of the increase of chitin microparticles loading on the mechanical properties of PLA.

Materials	Tensile strength (MPa)	Strain (%)
Neat PLA	41.5±0.8	9.0±0.7
PLA/1% chitin	44.3±1.3	7.8±0.9
PLA/2% chitin	46.1±1.1	6.3±1.5
PLA/3% chitin	48.9±0.7	4.8±1.2
PLA/4% chitin	45.5±0.5	4.4±1.3

Figure 6 shows the typical stress-strain curves of neat PLA and PLA/chitin composites with 1, 2, and 3% PLA loading. We limited the PLA loading to 3% as beyond that PLA loading the tensile strength started decreasing with further increase chitin loading. The neat PLA showed the lowest stress (41.7 MPa) at the highest strain (8.8%) but the PLA with 3% loading showed the highest stress (49.0 MPa) at the lowest strain (4.9%).
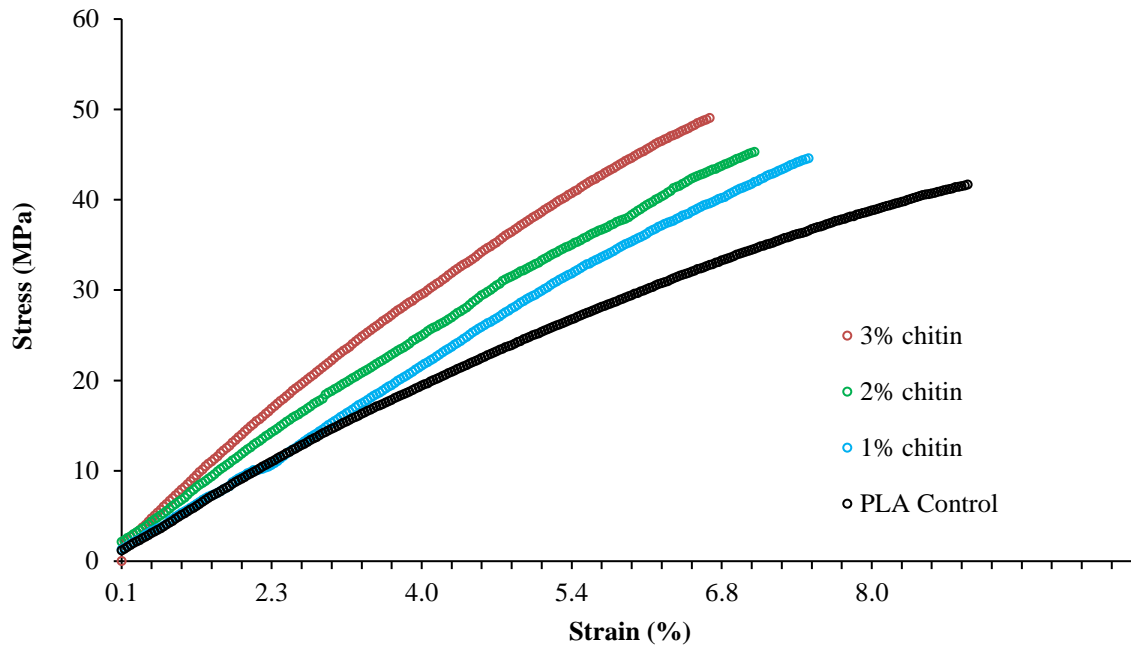
Figure 6 Stress-strain curves of neat PLA and PLA/chitin composites containing various weight (%) of chitin microparticles.

Surface and cross-sectional morphologies

Figure 7 shows the optical micrographs of neat PLA and PLA/chitin composite films containing 1, 2, and 3% PLA loading. It is evident that the density of chitin microparticles in the PLA composites increased with an increase in the PLA loading. It is also evident that chitin particles are uniformly distributed in the PLA matrix as no aggregation of chitin microparticles are visible, even at 3% chitin particle loading. The optical image also shows that the maximum length of the chitin particle in the composites is approximately 100 µm, which is consistent with the SEM image shown in Figure 1. There is debris of chitin visible in the composites, which indicates that chitin microparticles were further broken down into smaller particles during high-temperature melt compounding.
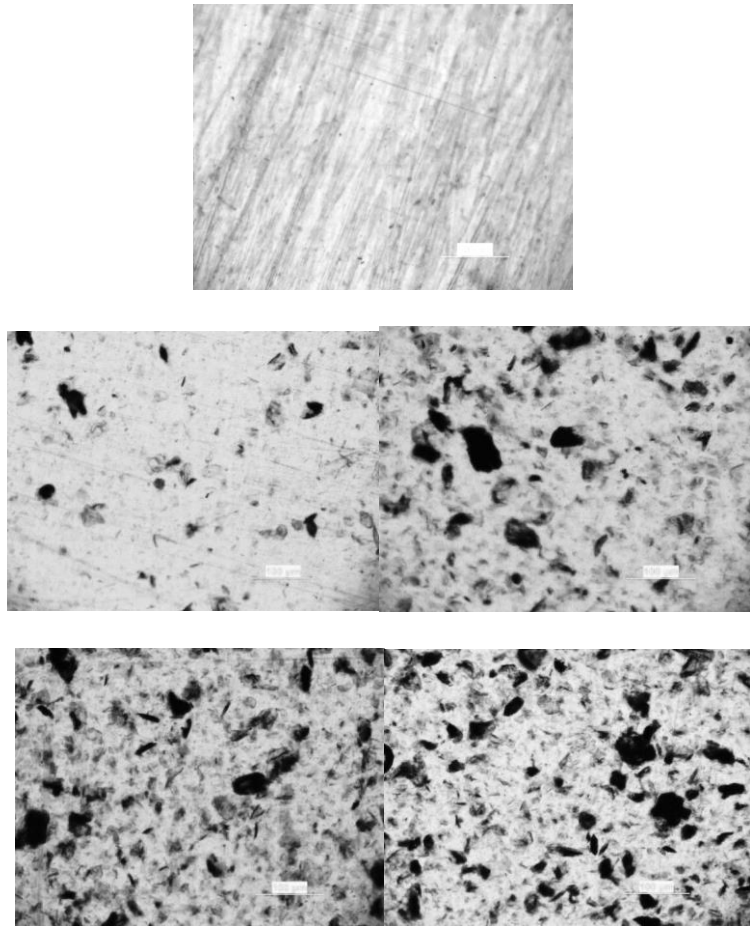
Figure 7   Optical images of surface of neat PLA film (a) and PLA/chitin biocomposite films containing 1 (b), 2 (c), 3% (d) and 4% (e) chitin loading.

The fractured surfaces of neat PLA and PLA/chitin composites were examined by the scanning electron microscopy to observe the effect of the addition of chitin to PLA on the microstructure of the PLA/chitin composites. The SEM image of neat PLA showed a brittle fracture pattern when it underwent an impact load as shown in Figure 8. Some areas are quite smooth, and some areas have some shallow but smooth groves, which is consistent with the inherent stiffness and brittle character of pristine PLA. Thus, it can be predicted that it has a low fractal dimension of surface morphology. On the other hand, the impact fractured surfaces of PLA/chitin microparticle composites were totally different from the surface of the pristine PLA as evident from SEM images shown in Figure 8. The fractured surface of

PLA/chitin microparticle composites became progressively rough with an increase in the chitin microparticle loading. However, the formation of pores and cracks is not evident from the SEM images, which is quite common for PLA/chitosan composites [36]. The chitin microparticles can be observed in the optical micrographs, especially for 3% chitin loading and they are bonded to the PLA matrix. The SEM images show that the chitin microfillers are compatible with the PLA matrix.
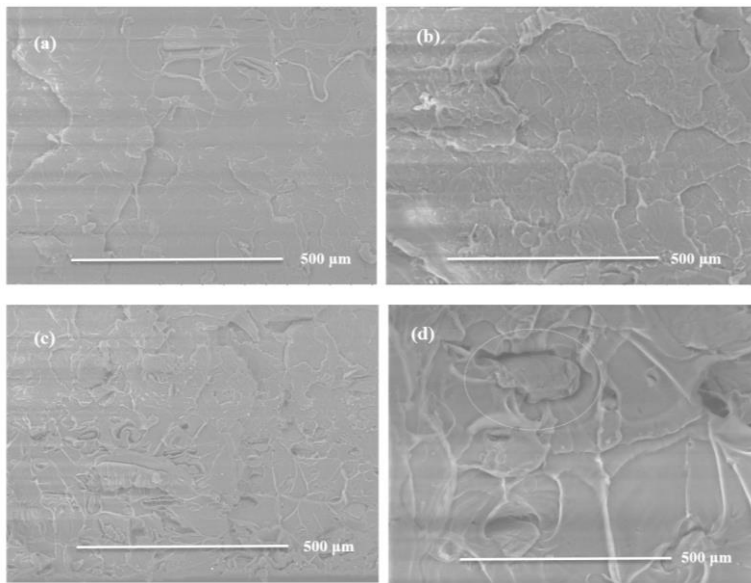

Figure 8   SEM micrographs of cracked surfaces of neat PLA and also PLA/chitin composites containing various chitin loading.

Water absorption

The water sorption behavior of plastic films is of fundamental importance for developing new packaging materials as the absorbed moisture may affect the shelf-life of the packaged food and may also enhance microbial growth. As chitin is quite hydrophobic, and therefore its addition to PLA may enhance its water absorbency.
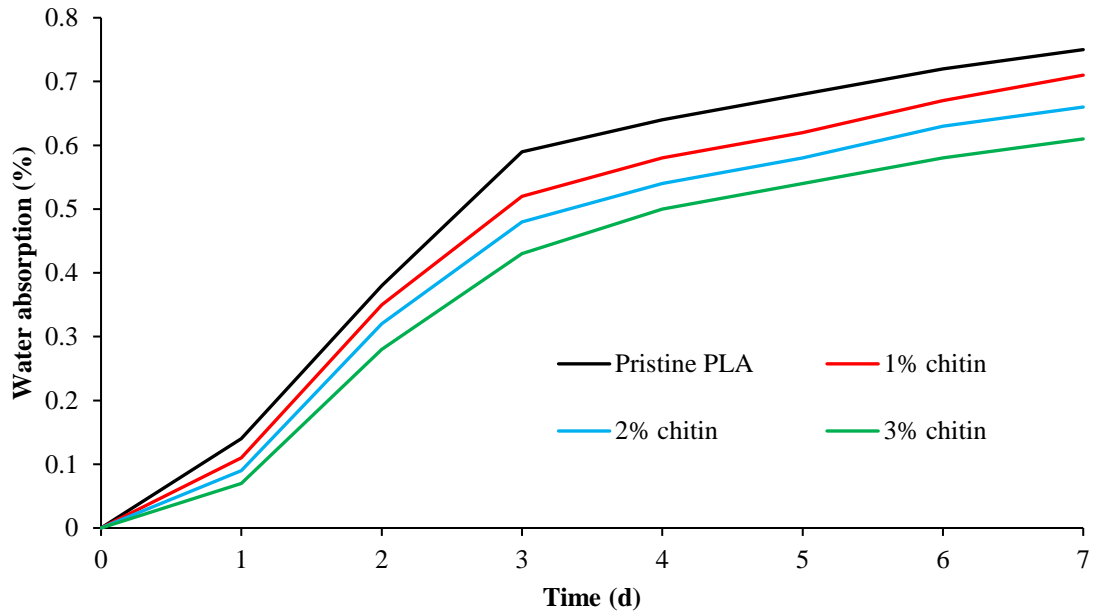
Figure 9   Water absorption curves of pristine PLA and PLA/chitin composites with 1, 2, and 3% PLA loading.

Figure 9 shows the water absorption curves of pristine PLA and PLA/chitin composite over 7 days. The pristine PLA absorbed little water on the first day and the maximum absorption occurred during the second to third days after which the absorption of water slowed down. The PLA composite containing various PLA loading also showed very similar behavior but showed considerably lower water absorption compared to the water absorbed by the pristine PLA. At 3 days of wetting time, the neat PLA showed a 0.6% water absorption. Conversely, the PLA with 3% chitin loading showed only 0.43% water absorption. After 7 days, the water absorption for the neat PLA reached 0.75% but the PLA with 3% loading showed only 0.6% water absorption. The results suggest that the hydrophobicity of PLA increased by the increase in chitin micro-particle loading.
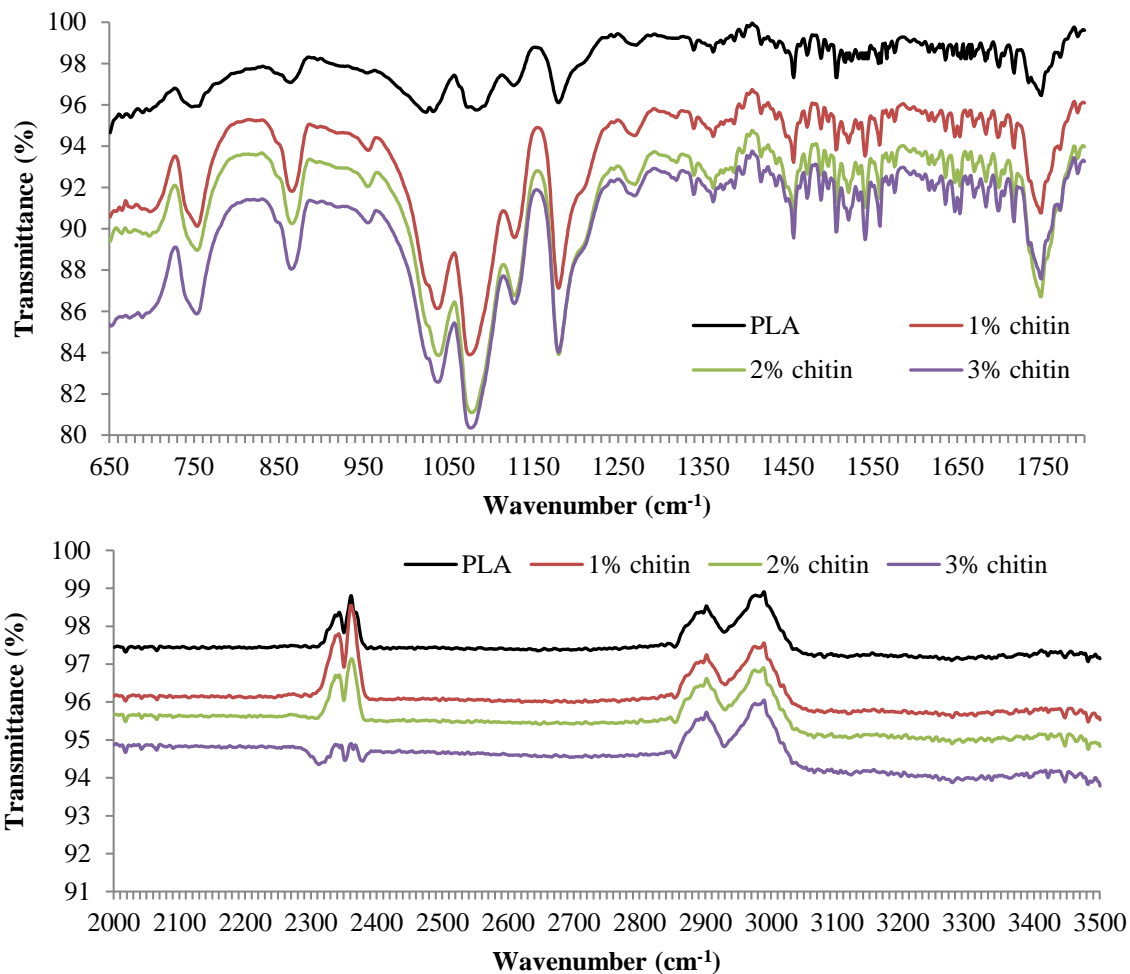
Figure 10   FTIR spectra of neat PLA and PLA/chitin biocomposites containing various

chitin microparticle loadings.

ATR-FTIR

Figure 10 shows the ATR-FTIR spectra of PLA and PLA/chitin composites with 1, 2, and 3%

PLA loading. In the spectrum of PLA, the strong IR band at 1749 cm^{-1} could be attributed to

the $-C=O$ stretching vibration of carbonyl groups ($-COOH$) of PLA, while the bending

vibrations of this group appear at 1270 cm^{-1}. The bands at 760, 867 and 1457 cm^{-1} represent

the crystalline and amorphous phases of PLA, and $-CH_3$ bending [37, 38]. The ATR-FTIR

spectra PLA/chitin also showed similar bands but the intensity of IR bands composites at

750, 860, 1032, 1070, 1178, 1746 increased and also moved slightly towards lower wavenumber compared to the control due to the interaction between PLA and chitin. The movement and intensity of various IR bands suggest that interaction occurred between the PLA matrix and the chitin microfillers.

Conclusions

The chitin microparticles used in this work were quite irregular in size and shape. We have demonstrated that chitin microparticles can be used as a filler in the fabrication of PLA/chitin biocomposites without using any compatibilizer or processing aid to reinforce the PLA films. The addition of chitin to PLA decreased the peak degradation temperature of PLA but increased the chard yield. Similarly, the addition of chitin microparticles increased the hydrophobicity of PLA by lowering the water absorption capacity and increased the stiffness and tensile strength of PLA. ATR-FTIR spectra confirm the interaction between PLA and chitin micro-fillers.

References

1.   Anand P, Rajesh D, Senthil Kumar M, Saran Raj I (2018) Investigations on the performances of treated jute/Kenaf hybrid natural fiber reinforced epoxy composite. *J Polym Res* 25:94.

2.   Qian X, Jin J, Lu L, Shao G, Jiang S (2017) Preparation of poly(methyl methacrylate) /silicon particle composites and the study of the properties improvement. *J Polym Res* 24:45.

3. Hassan M M, Le Guen M J, Tucker N, Parker K (2019) Thermo-mechanical, morphological and water absorption properties of thermoplastic starch/cellulose composite foams reinforced with PLA. *Cellulose* 26:4463–4478

4. Siddique R, Khatib J, Kaur I *(*2008) Use of recycled plastic in concrete: A review. *Waste Manag 28:*1835–1852.

5. Jambeck JR, Geyer R, Wilcox C, Siegler TR, Perryman M, Andrady A, Narayan R (2015), Plastic waste inputs from land into the ocean. Science 347:768–771

6. Cózar A, Echevarría F, González-Gordillo JI, Irigoien X, Úbeda B, Hernández-León S, Palma AT, Navarro S, García-de-Lomas J, Ruiz A, Fernández-de-Puelles ML, Duarte CM (2014), Plastic debris in the open ocean. Proc Nat Acad Sci 111:10239–10244.

7. Yang TH, Kim TW, Kang HO, Lee S-H, Lee EJ, Lim S-C, Oh SO, Song A-J, Park SJ, Lee SY (2010) Biosynthesis of polylactic acid and its copolymers using evolved propionate CoA transferase and PHA synthase. Biotechnol Bioeng 105:150–160.

8. Schmidt S, Scherkus C, Muschiol J, Menyes U, Winkler T, Hummel W, Gröger H, Liese A, Herz H-G, Bornscheuer UT (2015) An enzyme cascade synthesis of ε-caprolactone and its oligomers. Angewandte Chemie 54:2784–2787.

9. Labruyère C, Talon O, Berezina N, Khousakoun E, Jérôme C (2014) Synthesis of poly(butylene succinate) through oligomerization-cyclization- ROP route. RSC Adv 4:38643–38648.

10. Marang L, Jiang Y, van Loosdrecht MCM, Kleerebezem R (2013) Butyrate as preferred substrate for polyhydroxybutyrate production. Bioresour Technol 142:232–239.

11.   Wang Y, Chen R, Cai JY, Liu Z, Zheng Y, Wang H, Li Q, He N (2013) Biosynthesis and thermal properties of PHBV produced from levulinic acid by *Ralstonia eutropha*. PloS ONE 8:e60318

12.   Harris AM, Lee EC (2008) Improving mechanical performance of injection molded PLA by controlling crystallinity. J Appl Polym Sci 107:2246–2255.

13.   Mallet B, Lamnawar K, Maazouz A (2014) Improvement of blown film extrusion of poly(lactic acid): Structure-processing-properties relationships. Polym Eng Sci 54:840–857.

14.   Karkhanis SS, Stark NM, Sabo RC, Matuana LM (2017) Blown film extrusion of poly(lactic acid) without melt strength enhancers. J Appl Polym Sci 134:45212

15.   Zhang B, Seong B, Nguyen V, Byun D (2016) 3D printing of high-resolution PLA-based structures by hybrid electrohydrodynamic and fused deposition modeling techniques. J Micromechanics Microeng 26:025015

16.   Wang, H; Sun, X Z; Seib, P Strengthening blends of poly(lactic acid) and starch with methylene - diphenyl diisocyanate. J Appl Polym Sci 82 (2001) 1761.

17.   Frone AN, Berlioz S, Chailan JF, Panaitescu DM, Donescu D (2011) Cellulose fiber-reinforced polylactic acid. Polym Compos 32:976–985.

18.   Gherissi A, Cheikh RB, Dévaux E, Abbassi F (2012) Cellulose whiskers micro-fibers effect in the mechanical proprieties of PP and PLA composites fibers obtained by spinning process. Appl Mechanic Mater 146:12–26.

19.   Hassan MM, Koyama K (2015) Enhanced thermal, mechanical and fire-retarding properties of polystyrene sulphonate-grafted-nanosilica/polypropylene composites. RSC Adv 5:16950–16959.

20.   Muiruri JK, Liu S, Teo WS, Kong J, He C (2017) Highly biodegradable and tough polylactic acid-cellulose nanocrystal composite. ACS Sustain Chem Eng 5 3929–3937.

21.   Johari AP, Kurmvanshi SK, Mohanty S, Nayak SK (2016) Influence of surface modified cellulose microfibrils on the improved mechanical properties of poly (lactic acid). Int J Biologic Macromol 84:329–339.

22.   Qian S, Sheng K, Yu K, Xu L (2018) Fontanillo Lopez CA, Improved properties of PLA biocomposites toughened with bamboo cellulose nanowhiskers through silane modification. J Mater Sci 53:10920–10932.

23.   Yuryev Y, Mohanty AK, Misra M (2017) Novel durable biocomposites from biobased PC/PLA blend matrix system. Composites B 130:158–166.

24.   Gil-Castell O, Badia JD, Kittikorn T, Strömberg E, Ek M, Karlsson S, Ribes-Greus A (2016), Impact of hydrothermal aging on the thermal stability, morphology and viscoelastic performance of PLA/sisal biocomposites. Polym Degrad Stab 132:87–96.

25.   Cuevas-Carballo ZB, Duarte-Aranda S, Canché-Escamilla G (2017) Properties and biodegradability of thermoplastic starch obtained from granular starches grafted with polycaprolactone. Int J Polym Sci 2017:3975692.

26.   Weerapoprasit C, Prachayawarakorn J (2019) Characterization and properties of biodegradable thermoplastic grafted starch films by different contents of methacrylic acid. Int J Biologic Macromol 123:657–663.

27.   Modelli A, Rondinelli G, Scandola M, Mergaert J, Cnockaert MC (2004) Biodegradation of chemically modified flax fibers in soil and in vitro with selected bacteria. Biomacromolecules 5:596–602.

28. Singh AA, Wei J, Herrera N, Geng S, Oksman K (2018) Synergistic effect of chitin nanocrystals and orientations induced by solid-state drawing on PLA-based nanocomposite tapes. Compos Sci Technol 162:140–145.

29. Mahmoodi A, Ghodrati S, Khorasani M (2019) High-strength, low-permeable, and light-protective nanocomposite films based on a hybrid nanopigment and biodegradable PLA for food packaging applications. ACS Omega 4:14947–14954.

30. Lertphirun K, Srikulkit K ( ) Properties of poly(lactic acid) filled with hydrophobic cellulose/SiO$_2$ composites. Int J Polym Sci

31. Ahmed J, Varshney SK (2011) Polylactides-chemistry properties and green packaging technology: A review. Int J Food Prop 14:37–58.

32. Ca´rdenas G, Cabrera G, Taboada E, Miranda SP (2004) Chitin characterization by SEM, FTIR, XRD, and 13C cross polarization/mass angle spinning NMR. J Appl Polym Sci 93:1876–1885.

33. Duarte ML, Ferreira MC, Marvão MR, Rocha J (2002) An optimized method to determine the degree of acetylation of chitin and chitosan by FTIR spectroscopy. Int J Biological Macromol 31:1–8.

34. Cárdenas G, Cabrera G, Taboada E, Miranda SP (2004) Chitin characterization by SEM, FTIR, XRD, and13C cross polarization/mass angle spinning NMR. J Appl Polym Sci 93:1876–1885.

35. Chen P-Y, Lian H-Y, Shih Y-F, Chen-Wei S-M, Jeng R-J (2017) Preparation, characterization and crystallization kinetics of kenaf fiber/multi-walled carbon nanotube/polylactic acid (PLA) green composites. Mater Chem Phys 196:249–255.

36. Herrera N, Roch H, Salaberria AM, Pino-Orellana MA, Labidi J, Fernandes SCM, Radic D, Leiva A, Oksman K (2016) Functionalized blown films of plasticized

polylactic acid/chitin nanocomposite: Preparation and characterization. Mater Design 92: 846–852.

37. Spiridon I, Paduraru OM, Zaltariov MF, Darie RN (2013) Influence of keratin on polylactic acid/chitosan composite properties: Behavior upon accelerated weathering. Ind Eng Chem Res 52:9822–9833.

38. Rocca-Smith JR, Lagorce-Tachon A, Iaconelli C, Bellat JP, Marcuzzo E, Sensidoni A, Piasente F, Debeaufort F, Karbowiak T (2017) How high-pressure CO_2 impacts PLA film properties. Express Polym Lett 11:320–333.